PERGAMON

International Journal of Solids and Structures 39 (2002) 3109–3130

INTERNATIONAL JOURNAL OF SOLIDS and STRUCTURES

www.elsevier.com/locate/ijsolstr

Limit angular velocities of variable thickness rotating disks

Ahmet N. Eraslan *, Hakan Argeso

Department of Engineering Sciences, Middle East Technical University, Ankara 06531, Turkey

Received 4 October 2001; received in revised form 13 March 2002

Abstract

Elastic and plastic limit angular velocities are calculated for rotating disks of variable thickness in power function form. Analytical solution is obtained and used to calculate elastic limit angular velocities of variable thickness rotating annular disks and annular disks with rigid inclusion. An efficient numerical solution procedure is designed and used to obtain the elastic limit angular velocities of variable thickness rotating solid disks. Von Mises yield criterion and its flow rule is used to estimate plastic limit angular velocities. Both linear and nonlinear hardening material behaviors are treated numerically. The results are verified by comparing with those of uniform thickness rotating solid disks available in the literature. Elastic and plastic limit angular velocities are found to increase with the reduction of the disk thickness at the edge as well as the reduction in the disk mass due to the shape of the profile.

Keywords: Stress analysis; Rotating disks; Variable thickness; Nonlinear strain hardening

1. Introduction

Estimation of elastic and especially plastic limit angular velocities in the design of disks rotating at high speeds is an important subject due to a large number of applications in mechanical engineering. For this reason, the theoretical investigation of stresses and displacement in such structures has been receiving considerable attention and the topic was discussed in many standard textbooks (Calladine, 1969; Timoshenko and Goodier, 1970; Rees, 1990). The majority of the work in the area considers constant thickness rotating solid or annular disks and uses Tresca's yield condition and flow rule. Relatively fewer articles exist in the literature employing von Mises yield criterion and its flow rule mainly because of the nonlinearities inherent in this criterion. Among the numerous articles reporting the results of research conducted on the subject, the most recent ones relevant to this investigation are reviewed below.

You et al. (1997, 1999) proposed a perturbation method and a power series method of solution for estimating elastoplastic deformations of rotating uniform thickness disks. They employed von Mises yield condition combined with a polynomial yield stress-equivalent strain relation, which describes nonlinear hardening material behavior. Elastic–plastic stresses and displacement in a uniform thickness disk have

* Corresponding author. Address: Müh. Bil. Böl., ODTU, Ankara 06531, Turkey. Fax: +90-312-210-1269.
E-mail address: aeraslan@metu.edu.tr (A.N. Eraslan).

0020-7683/02/$ - see front matter
PII: S0020-7683(02)00249-4

been computed. The validity of the perturbation solution technique to handle the nonlinearity associated with von Mises yield condition and assumed polynomial stress–strain relationship has been demonstrated by comparison with finite element solution and analytical solution which uses Tresca's yield condition. An extension of this work was conducted by You et al. (2000) that combines this model with a Runge–Kutta numerical solution procedure to compute elastic–plastic stresses in rotating disks of variable thickness and density. The results reported by them concentrated on variable thickness and variable density annular disks but the results of variable thickness solid disks were not presented.

Tresca's yield condition and its associated flow rule was compared with von Mises criterion and flow rule in estimating elastic–plastic and residual stresses of rotating constant thickness solid and annular disks by Rees (1999). It is shown that for uniform thickness disks von Mises solution simplifies to a form which is appropriate for Runge–Kutta solution, by the use of standard elliptical substitutions. Tresca's yield condition has been found to predict slightly lower limit angular velocities than that of von Mises.

The stresses and deformations of rotating constant and linearly varying thickness solid and annular disks were studied by Ma et al. (2001). They used a unified yield criterion such that one of Tresca, von Mises or Yu criterion could be obtained by a suitable adjustment of the weighting coefficient. Two of their results for rotating solid and annular disks with a linear disk profile in the form $h(r) = 3 - 2r$ are compared with those obtained in this work in the following sections. However, the constant radial and circumferential stresses obtained by Ma et al. in the central portion of the disks fail to satisfy the equation of motion.

The stresses in the rotating hyperbolic disk with rigid inclusion were studied analytically by Güven (1998) using Tresca's yield condition, its flow rule and linear hardening. The stresses in such variable thickness disks have been found to be affected by the thickness parameter that defines the shape of the disk profile.

In a recent work, Eraslan and Orcan (2002) studied elastic–plastic deformations of rotating solid disks of exponentially varying thickness. An analytical solution has been obtained using Tresca's yield condition and its associated flow rule for linearly strain hardening. Their analysis indicated that, unlike constant thickness disks, for steep disk profiles the radial stress at the central core exceeds circumferential stress. Accordingly, the plastic zone develops away from the axis of the disk and propagates in all radial directions.

There appears only a few number of work in the literature investigating inelastic deformations of variable thickness rotating disks using von Mises yield condition combined with nonlinear hardening. This work attempts to perform a comprehensive study on inelastic as well as elastic deformations of variable thickness annular and solid disks rotating at high speeds.

2. Elastic solution and elastic limit angular velocities

The disk is symmetric with respect to the mid-plane and its thickness varies according to

$$\bar{h}(\bar{r}) = (1 - n\bar{r})^k \tag{2.1}$$

in which $\bar{h} = h/h_0$ is the dimensionless thickness, h_0 thickness at the axis of the disk, $\bar{r} = r/b$ dimensionless radial coordinate, b radius of the disk, n and k are dimensionless thickness parameters. The thickness of the disk is assumed to be sufficiently small compared to its diameter so that plane stress assumption is justified. With this form of the disk profile function, uniform thickness disk can be obtained by setting either $n = 0$ or $k = 0$ and a linearly decreasing thickness can be obtained by simply setting $k = 1$. Furthermore, if $k < 1$ the profile is convex and it is concave if $k > 1$.

A state of plane stress ($\sigma_z = 0$) and infinitesimal deformations are presumed. Using the formal dimensionless variables: dimensionless stress $\bar{\sigma}_{ij} = \sigma_{ij}/\sigma_0$ and dimensionless angular velocity $\Omega = \omega b\sqrt{\rho/\sigma_0}$, the equation of motion in dimensionless form reads

$$\frac{\mathrm{d}}{\mathrm{d}\bar{r}}(\bar{h}\bar{r}\bar{\sigma}_{\mathrm{r}}) - \bar{h}\bar{\sigma}_{\theta} + \bar{h}\Omega^2\bar{r}^2 = 0 \tag{2.2}$$

where σ_0 stands for the yield limit, ω constant angular velocity and ρ mass density. The geometric relations are

$$\bar{\epsilon}_{\theta} = \frac{\bar{u}}{\bar{r}} \tag{2.3}$$

$$\bar{\epsilon}_{\mathrm{r}} = \frac{\mathrm{d}\bar{u}}{\mathrm{d}\bar{r}} \tag{2.4}$$

in which $\bar{u} = uE/b\sigma_0$ is the dimensionless displacement, $\bar{\epsilon}_{\mathrm{ij}} = \epsilon_{\mathrm{ij}}E/\sigma_0$ the normalized strain, u the displacement, and E the modulus of elasticity. It should be noted that the equation of motion and strain-displacement relations holds irrespective of material behavior. In Eqs. (2.3) and (2.4) $\bar{\epsilon}_{\mathrm{ij}}$ represents total mechanical strains given by

$$\bar{\epsilon}_{\mathrm{ij}} = \bar{\epsilon}^{\mathrm{e}}_{\mathrm{ij}} + \bar{\epsilon}^{\mathrm{p}}_{\mathrm{ij}} \tag{2.5}$$

where the superscripts e and p are used to indicate elastic and plastic counterparts of the total strain, respectively. For purely elastic deformations of the disk

$$\bar{\epsilon}_{\mathrm{r}} = \bar{\epsilon}^{\mathrm{e}}_{\mathrm{r}} = \bar{\sigma}_{\mathrm{r}} - v\bar{\sigma}_{\theta} \tag{2.6}$$

$$\bar{\epsilon}_{\theta} = \bar{\epsilon}^{\mathrm{e}}_{\theta} = \bar{\sigma}_{\theta} - v\bar{\sigma}_{\mathrm{r}} \tag{2.7}$$

in which v is the Poisson ratio. A stress function formulation and analytical solution for annular disks are given below. The displacement formulation and the solution are presented in Appendix A.

Defining the dimensionless stress function in terms of radial stress (Timoshenko and Goodier, 1970)

$$Y(\bar{r}) = \bar{h}\bar{r}\bar{\sigma}_{\mathrm{r}} \tag{2.8}$$

from which

$$\bar{\sigma}_{\mathrm{r}} = \frac{Y}{\bar{h}\bar{r}} \tag{2.9}$$

Substituting Eq. (2.9) in Eq. (2.2) the circumferential stress is obtained as

$$\bar{\sigma}_{\theta} = \Omega^2\bar{r}^2 + \frac{1}{\bar{h}}\frac{\mathrm{d}Y}{\mathrm{d}\bar{r}} \tag{2.10}$$

The radial and circumferential stresses defined in this manner automatically satisfy the equation of motion, given by Eq. (2.2). Elastic strains can be rewritten in terms of the stress function Y as

$$\bar{\epsilon}_{\mathrm{r}} = \frac{Y}{\bar{h}\bar{r}} - v\left[\Omega^2\bar{r}^2 + \frac{1}{\bar{h}}\frac{\mathrm{d}Y}{\mathrm{d}\bar{r}}\right] \tag{2.11}$$

$$\bar{\epsilon}_{\theta} = \Omega^2\bar{r}^2 + \frac{1}{\bar{h}}\frac{\mathrm{d}Y}{\mathrm{d}\bar{r}} - v\left[\frac{Y}{\bar{h}\bar{r}}\right] \tag{2.12}$$

Substituting the elastic strains from Eqs. (2.11) and (2.12) in the compatibility relation

$$\frac{\mathrm{d}}{\mathrm{d}\bar{r}}(\bar{r}\bar{\epsilon}_{\theta}) - \bar{\epsilon}_{\mathrm{r}} = 0 \tag{2.13}$$

the following differential equation in terms of the stress function $Y(\bar{r})$ is obtained.

$$\frac{\mathrm{d}^2Y}{\mathrm{d}\bar{r}^2}+\left[\frac{1}{\bar{r}}-\frac{\bar{h}'}{\bar{h}}\right]\frac{\mathrm{d}Y}{\mathrm{d}\bar{r}}+\left[-\frac{1}{\bar{r}^2}+\frac{v\bar{h}'}{\bar{r}\bar{h}}\right]Y=f(\bar{r}) \tag{2.14}$$

where a prime denotes differentiation with respect to radial coordinate $\bar{r}$, and

$$f(\bar{r})=-(3+v)\bar{h}\Omega^2\bar{r} \tag{2.15}$$

Hence, the homogeneous equation corresponds to $f(\bar{r})=0$. The boundary conditions for Y are to be obtained from the boundary conditions for the stresses which are given as follows:

I Solid disks

$$\bar{\sigma}_{\mathrm{r}}(0)=\bar{\sigma}_{\theta}(0)\quad\text{and}\quad\bar{\sigma}_{\mathrm{r}}(1)=0 \tag{2.16}$$

II Annular disks

$$\bar{\sigma}_{\mathrm{r}}(\bar{r}_0)=0\quad\text{and}\quad\bar{\sigma}_{\mathrm{r}}(1)=0 \tag{2.17}$$

III Annular disks with rigid inclusion

$$\bar{\sigma}_{\theta}(\bar{r}_0)-v\bar{\sigma}_{\mathrm{r}}(\bar{r}_0)=0\quad\text{and}\quad\bar{\sigma}_{\mathrm{r}}(1)=0 \tag{2.18}$$

where $\bar{r}_0$ is the inner radius of the disk. The last condition above is obtained by making use of the fact that at the rigid inclusion–disk contact area the radial displacement vanishes. If $\bar{h}=(1-n\bar{r})^k$ and $\bar{h}'=-kn(1-n\bar{r})^{k-1}$ are substituted in Eq. (2.14) one solution to the homogeneous equation is obtained as

$$y_1(\bar{r})=\bar{r}\mathsf{F}(a,b,c,n\bar{r}) \tag{2.19}$$

where $\mathsf{F}(\alpha,\beta,\gamma,x)$ is the hypergeometric function given by (Abramowitz and Stegun, 1966)

$$\mathsf{F}(\alpha,\beta,\gamma,x)=1+\frac{\alpha\beta}{\gamma 1!}x+\frac{\alpha(\alpha+1)\beta(\beta+1)}{\gamma(\gamma+1)2!}x^2+\frac{\alpha(\alpha+1)(\alpha+2)\beta(\beta+1)(\beta+2)}{\gamma(\gamma+1)(\gamma+2)3!}x^3+\cdots \tag{2.20}$$

The series $\mathsf{F}(\alpha,\beta,\gamma,x)$ converges slowly for $|x|<1$ provided that $\gamma-(\alpha+\beta)>-1$. Since the problem under consideration is a realistic physical problem, these conditions are always satisfied and the series is always convergent. The arguments a, b and c of the hypergeometric function F in Eq. (2.19) have the following meanings:

$$\begin{aligned}a&=1-\frac{k}{2}-\frac{1}{2}\sqrt{k^2+4(1-kv)}\\ b&=1-\frac{k}{2}+\frac{1}{2}\sqrt{k^2+4(1-kv)}\\ c&=3\end{aligned} \tag{2.21}$$

The second linearly independent solution is obtained by assuming that the homogeneous solution is in the form $Y(\bar{r})=y_1(\bar{r})\cdot V(\bar{r})$. Substituting in the homogeneous equation gives

$$y_1\frac{\mathrm{d}^2V}{\mathrm{d}\bar{r}^2}+\left\{y_1\left[\frac{1}{\bar{r}}-\frac{\bar{h}'}{\bar{h}}\right]+2\frac{\mathrm{d}y_1}{\mathrm{d}\bar{r}}\right\}\frac{\mathrm{d}V}{\mathrm{d}\bar{r}}=0 \tag{2.22}$$

The solution is

$$V(\bar{r})=C_1+C_2I_1(\bar{r}) \tag{2.23}$$

where

$$I_1(\bar{r}) = \int_{\bar{r}_0}^{\bar{r}} \frac{\bar{h}(\xi)}{\xi y_1(\xi)^2} \mathrm{d}\xi \tag{2.24}$$

Therefore, the second solution for $Y(\bar{r})$ is found to be

$$y_2(\bar{r}) = y_1(\bar{r}) I_1(\bar{r}) \tag{2.25}$$

For solid disks $\bar{r}_0 = 0$, the integral in Eq. (2.24) contains non-integrable singularity at the axis of the disk. Hence, the solution presented herein is valid for annular disks.

The general solution for $Y(\bar{r})$ is obtained as

$$Y(\bar{r}) = C_1 y_1(\bar{r}) + C_2 y_2(\bar{r}) + R(\bar{r}) \tag{2.26}$$

in which $R(\bar{r})$ is the particular solution in the form

$$R(\bar{r}) = u_1(\bar{r}) y_1(\bar{r}) + u_2(\bar{r}) y_2(\bar{r}) \tag{2.27}$$

with

$$u_1(\bar{r}) = -\int_{\bar{r}_0}^{\bar{r}} \frac{y_2(z) f(z)}{W_r(z)} \mathrm{d}z \quad \text{and} \quad u_2(\bar{r}) = \int_{\bar{r}_0}^{\bar{r}} \frac{y_1(z) f(z)}{W_r(z)} \mathrm{d}z \tag{2.28}$$

The Wronskian $W_r(\bar{r})$ is

$$W_r(\bar{r}) = y_1 \frac{\mathrm{d}y_2}{\mathrm{d}\bar{r}} - y_2 \frac{\mathrm{d}y_1}{\mathrm{d}\bar{r}} = \frac{\bar{h}(\bar{r})}{\bar{r}} \tag{2.29}$$

Hence, the general solution becomes

$$Y(\bar{r}) = y_1(\bar{r}) \Big[C_1 + C_2 I_1(\bar{r}) + I_1(\bar{r}) I_2(\bar{r}) - I_3(\bar{r}) \Big] \tag{2.30}$$

in which

$$I_2(\bar{r}) = \int_{\bar{r}_0}^{\bar{r}} \frac{z y_1(z) f(z)}{\bar{h}(z)} \mathrm{d}z \tag{2.31a}$$

$$I_3(\bar{r}) = \int_{\bar{r}_0}^{\bar{r}} \int_{\bar{r}_0}^{z} \left[\frac{z y_1(z) f(z)}{\bar{h}(z)} \right] \left[\frac{\bar{h}(\xi)}{\xi y_1(\xi)^2} \right] \mathrm{d}\xi \, \mathrm{d}z \tag{2.31b}$$

The analytical solution is completed by the application of the boundary conditions. For the annular disk the result is

$$C_1 = 0 \text{ and } C_2 = -I_2(1) + \frac{I_3(1)}{I_1(1)} \tag{2.32}$$

For the annular disk with rigid inclusion the integration constants are evaluated as

$$C_1 = \frac{\bar{h}(\bar{r}_0) \Big\{ I_3(1) + I_1(1) \Big[\bar{r}_0^3 \Omega^2 y_1(\bar{r}_0) - I_2(1) \Big] \Big\}}{\bar{h}(\bar{r}_0) + I_1(1) y_1(\bar{r}_0) \Big[\nu y_1(\bar{r}_0) - \bar{r}_0 y_1'(\bar{r}_0) \Big]} \tag{2.33}$$

$$C_2 = \frac{y_1(\bar{r}_0) \Big\{ -\bar{r}_0^3 \Omega^2 \bar{h}(\bar{r}_0) + [I_3(1) - I_1(1) I_2(1)] \Big[\nu y_1(\bar{r}_0) - \bar{r}_0 y_1'(\bar{r}_0) \Big] \Big\}}{\bar{h}(\bar{r}_0) + I_1(1) y_1(\bar{r}_0) \Big[\nu y_1(\bar{r}_0) - \bar{r}_0 y_1'(\bar{r}_0) \Big]} \tag{2.34}$$

in which the derivative y_1' is

$$\frac{dy_1}{d\bar{r}} = \mathsf{F}(a,b,c,n\bar{r}) + \frac{\bar{r}abn}{c}\mathsf{F}(a+1,b+1,c+1,n\bar{r})$$

An alternate analytical solution for this stress function formulation is given in Appendix B. Once the solution is found in terms of Y, the stresses are obtained from

$$\bar{\sigma}_r(\bar{r}) = \frac{y_1}{\bar{h}\bar{r}}\left[C_1 + C_2 I_1(\bar{r}) + I_1(\bar{r})I_2(\bar{r}) - I_3(\bar{r})\right] \tag{2.35}$$

$$\bar{\sigma}_\theta(\bar{r}) = \Omega^2\bar{r}^2 + \frac{1}{\bar{h}}\frac{dy_1}{d\bar{r}}\left[C_1 + C_2 I_1(\bar{r}) + I_1(\bar{r})I_2(\bar{r}) - I_3(\bar{r})\right] + \frac{y_1}{\bar{h}}\left[C_2\frac{dI_1}{d\bar{r}} + \frac{dI_1}{d\bar{r}}I_2(\bar{r}) + I_1(\bar{r})\frac{dI_2}{d\bar{r}} - \frac{dI_3}{d\bar{r}}\right] \tag{2.36}$$

where

$$\frac{dI_1}{d\bar{r}} = \frac{\bar{h}(\bar{r})}{\bar{r}y_1(\bar{r})^2} \tag{2.37a}$$

$$\frac{dI_2}{d\bar{r}} = \frac{\bar{r}y_1(\bar{r})f(\bar{r})}{\bar{h}(\bar{r})} \tag{2.37b}$$

$$\frac{dI_3}{d\bar{r}} = \frac{dI_2}{d\bar{r}}\cdot I_1(\bar{r}) \tag{2.37c}$$

Since the closed form solution cannot be found for a solid disk, its solution will be obtained by numerical means. For this aim, Eq. (2.14) is put into the general form

$$\frac{d^2Y}{d\bar{r}^2} = f\left(\bar{r}, Y, \frac{dY}{d\bar{r}}\right) \tag{2.38}$$

Letting $\phi_1 = Y$ and $\phi_2 = dY/d\bar{r}$, Eq. (2.38) is converted into a system of initial value problems

$$\frac{d\phi_1}{d\bar{r}} = \phi_2 \tag{2.39}$$

$$\frac{d\phi_2}{d\bar{r}} = f(\bar{r},\phi_1,\phi_2) \tag{2.40}$$

subject to the initial conditions

$$\phi_1^0 = Y(0) \text{ and } \phi_2^0 = \left.\frac{dY}{d\bar{r}}\right|_{\bar{r}=0} \tag{2.41}$$

From Eq. (2.8) $\phi_1^0 = 0$, but ϕ_2^0 is not known. To find out this unknown initial condition a Newton iteration scheme can be set up by requiring that $Y(1) = 0$.

First, the elastic limit angular velocity is calculated for a uniform thickness annular disk having an inner radius of $\bar{r}_0 = 0.1$ using $\nu = 1/3$. The non-zero integration constant is found to be $C_2 = 9.683623 \times 10^{-3}$ and the corresponding elastic limit angular velocity is calculated as $\Omega_1 = 1.094351$. The stresses and displacement at this limit angular velocity are displayed in Fig. 1. As seen in this figure, for rotating uniform thickness annular disks, the circumferential stress is the largest principal stress which reaches its maximum value at the inner surface, $\bar{r} = \bar{r}_0$. Variable thickness annular disk calculations are then performed by setting $\bar{r}_0 = 0.1$ and $k = 1$ and using the elastic limit angular velocity of the uniform thickness disk, $\Omega_1 = 1.094351$.

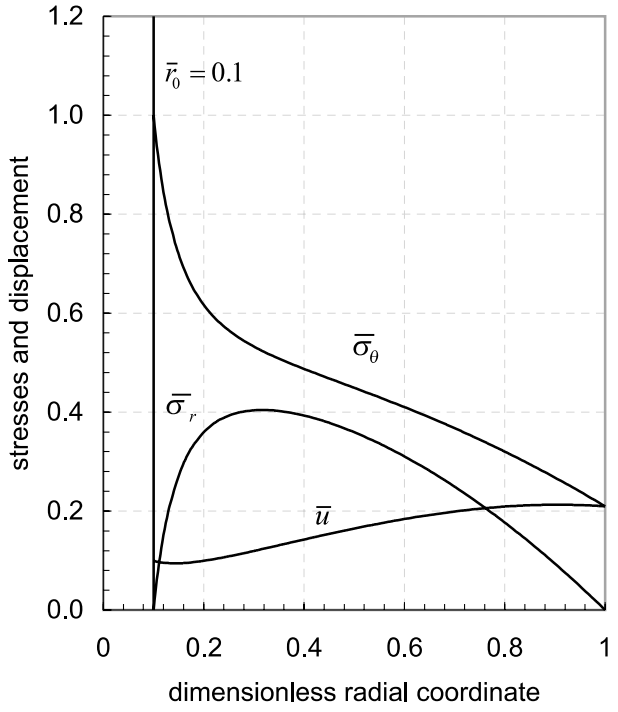

Fig. 1. Elastic stresses and displacement in rotating constant thickness annular disk of inner radius $\bar{r}_0 = 0.1$ at the elastic limit angular velocity $\Omega_1 = 1.094351$.

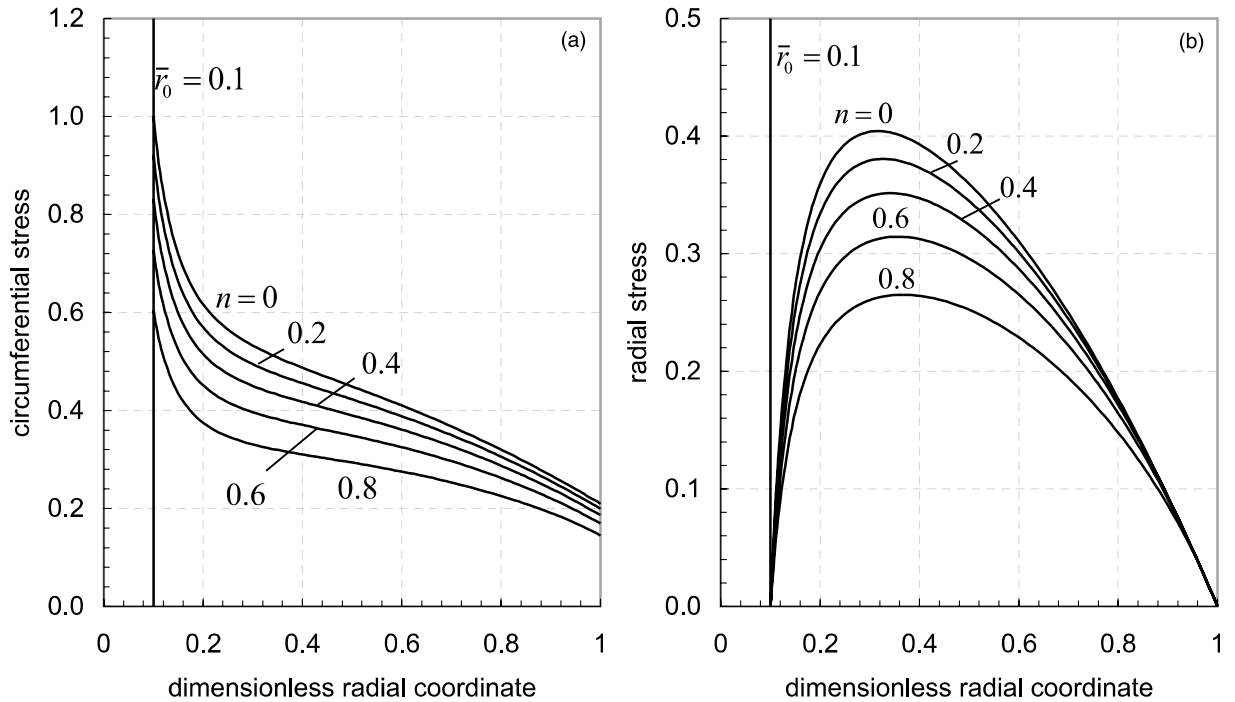

Fig. 2. Comparison of (a) elastic circumferential stresses (b) elastic radial stresses in rotating variable thickness annular disks of inner radius $\bar{r}_0 = 0.1$ at the elastic limit angular velocity $\Omega_1 = 1.094351$.

The results of these calculations are compared with those of uniform thickness disk in Fig. 2(a) and (b). Fig. 2(a) compares circumferential stresses of uniform and variable thickness disks by changing the geometric parameter n. As seen in this figure, all curves have similar shape. At the elastic limit angular velocity the largest circumferential stress occurs in uniform thickness disk and as the reduction of the disk thickness at the edge decreases the stresses decrease as well. The smallest stress corresponds to the largest decrease in the disk thickness. Fig. 2(b) compares radial stresses of uniform and variable thickness disks. Again, the largest radial stress occurs in uniform thickness disk, the smallest corresponds to 80% decrease in disk thickness at the edge of the disk. Variation of the elastic limit angular velocity with the geometric parameter n for $k = 1$ is calculated and plotted in Fig. 3 for annular disks with inner radius $\bar{r}_0 = 0.1$, 0.2, 0.3 and 0.4. In each disk $n = 0$ corresponds to uniform thickness disk. Elastic limit angular velocities increase as the reduction in the disk thickness increases. The largest elastic limit angular velocities correspond to the annular disk with the smallest inner radius. As the inner radius increases elastic limit angular velocities decrease.

Taking $\bar{r}_0 = 0.1$ and $\nu = 1/3$ the elastic limit angular velocity of a uniform thickness annular disk with rigid inclusion is calculated. The integration constants are found to be $C_1 = 9.8 \times 10^{-1}$ and $C_2 = -6.692874 \times 10^{-3}$ and the elastic limit angular velocity is calculated as $\Omega_1 = 1.273185$. The corresponding stresses and displacement are shown in Fig. 4. In contrast to the annular disk, the radial stress is the largest stress in this disk and its maximum value is at the rigid inclusion–annular disk interface. The radial and circumferential stresses at $\Omega_1 = 1.273185$ are compared with those of linearly varying thickness disks of different thickness reduction in Fig. 5(a) and (b). Both radial and circumferential stresses indicate similar behavior and the largest stresses are those of uniform thickness annular disk with rigid inclusion. The effect of the reduction in disk thickness on elastic limit angular velocities is illustrated in Fig. 6 using inner radius $\bar{r}_0$ as a parameter. As in annular disks, the limit angular velocity increases with increasing thickness reduction for each disk. For annular disks with rigid inclusion, elastic limit angular velocities

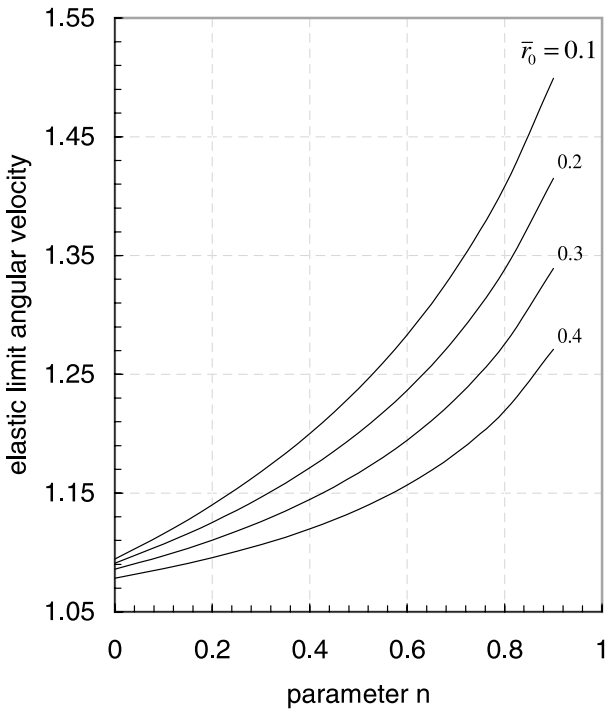

Fig. 3. Variation of elastic limit angular velocity with the thickness reduction for rotating variable thickness annular disks.

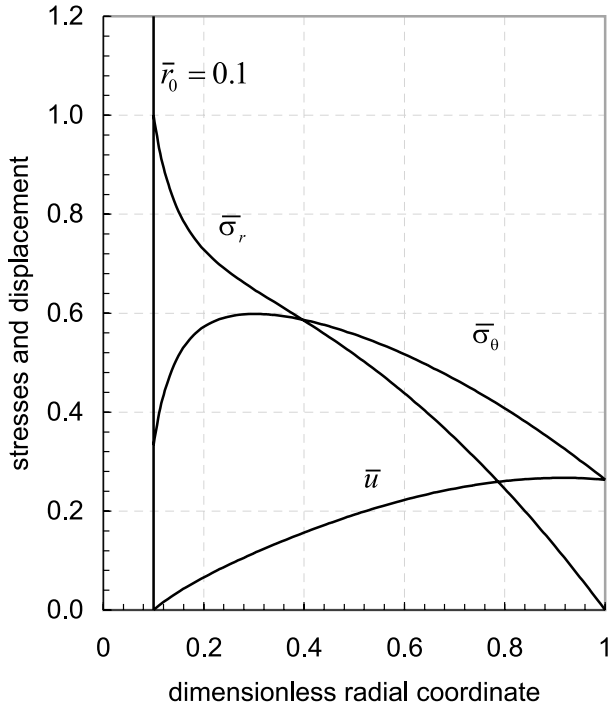

Fig. 4. Elastic stresses and displacement in rotating constant thickness annular disk with rigid inclusion having an inner radius $\bar{r}_0 = 0.1$ at the elastic limit angular velocity $\Omega_1 = 1.273185$.

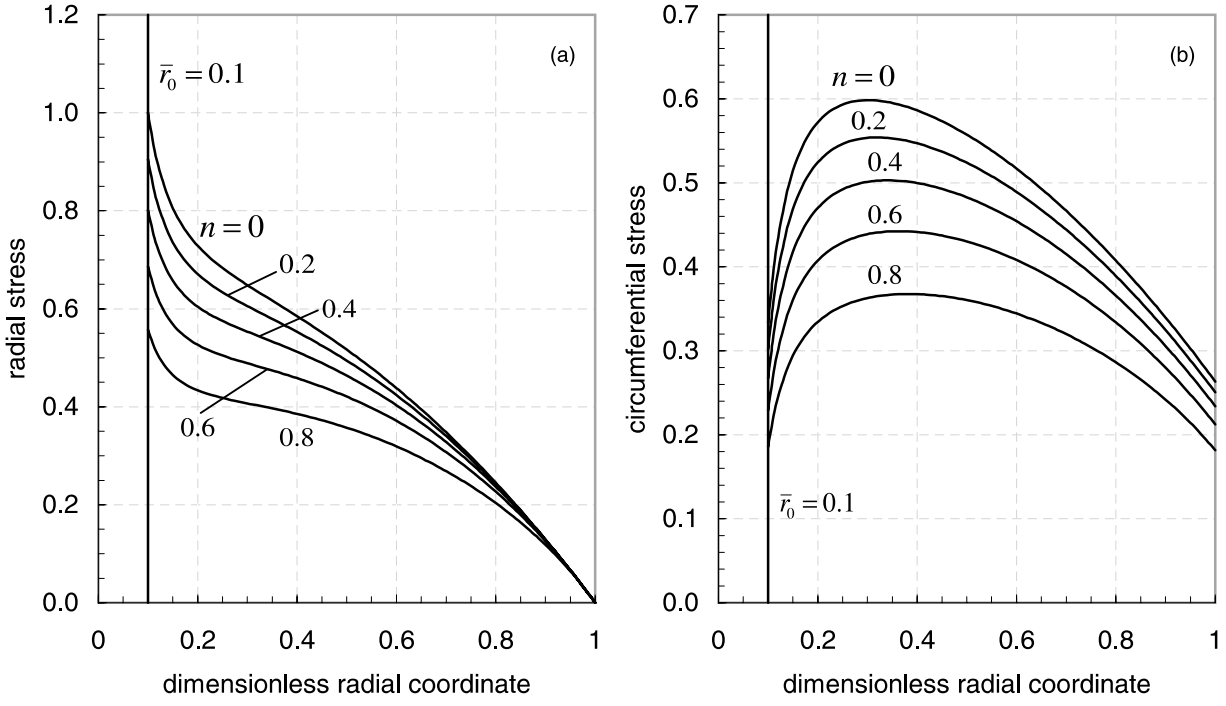

Fig. 5. Comparison of (a) elastic radial stresses (b) elastic circumferential stresses in rotating variable thickness annular disks with rigid inclusion having an inner radius of $\bar{r}_0 = 0.1$ at the elastic limit angular velocity $\Omega_1 = 1.273185$.

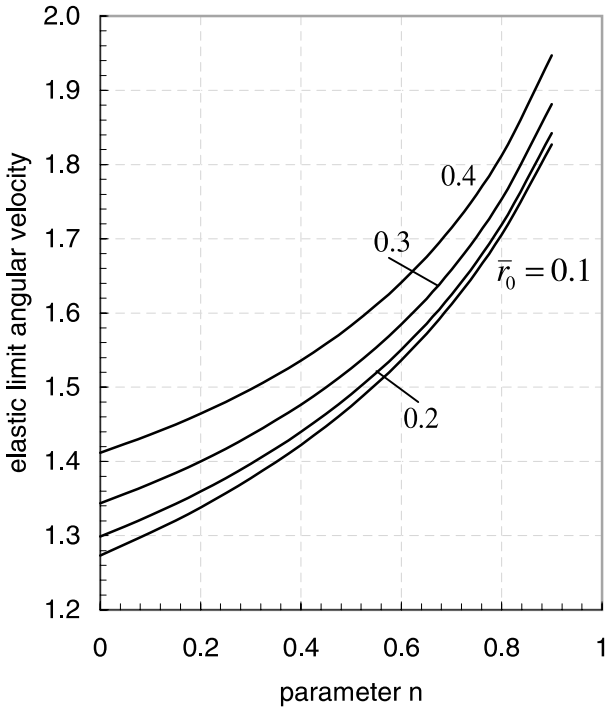

Fig. 6. Variation of elastic limit angular velocity with the thickness reduction for rotating variable thickness annular disks with rigid inclusion.

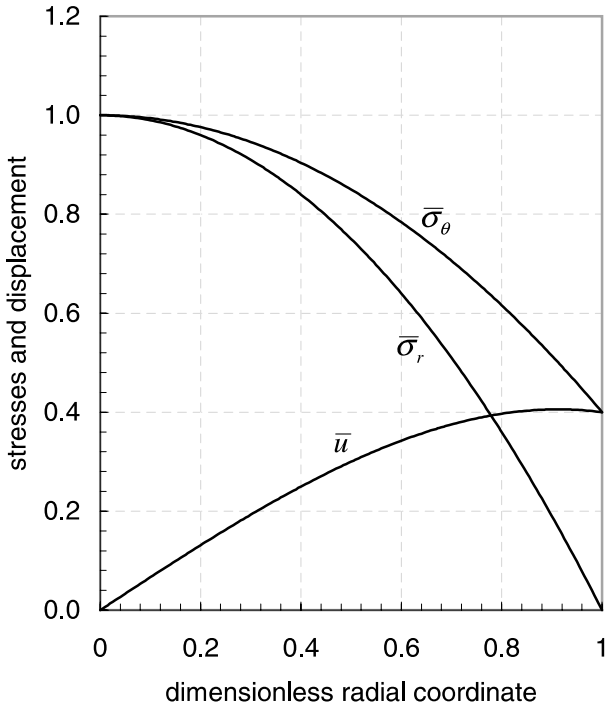

Fig. 7. Elastic stresses and displacement in rotating constant thickness solid disk at the elastic limit angular velocity $\Omega_1 = 1.549193$.

increase as $\bar{r}_0$ increases. This is as expected because if the disk were entirely rigid, the elastic limit angular velocity would tend to infinity.

The numerical solution procedure for variable thickness solid disks, as described above, is verified by comparison with the analytical solution. For this purpose, the elastic limit angular velocity of uniform thickness disk is computed by setting $v = 1/3$ and $n = 0$. The elastic limit angular velocity is reached in five main iterations to hit $\bar{\sigma}_r(0) = \bar{\sigma}_\theta(0) = 1.0$ and on the average 5 Newton iterations required in each to determine $dY/d\bar{r}|_{\bar{r}=0}$. The elastic limit angular velocity is obtained as $\Omega_1 = 1.549193$. Gamer (1984) reports this as $\Omega_1 = 1.54919$ by carrying out an analytical solution for a rotating constant thickness solid disk. The limit angular velocity calculated in this work agrees with Gamer's result in all the digits as reported. The corresponding stresses and displacement are plotted in Fig. 7 showing well-known stress displacement distributions of uniform thickness solid disks. The circumferential stress is the largest stress throughout the disk and both stresses reach their maximum at the axis. It is also typical that if the Poisson ratio is taken as $1/3$, the dimensionless circumferential stress becomes exactly equal to the dimensionless displacement at the edge of the disk.

To find out the elastic deformation behavior of variable thickness rotating solid disks three different profiles are chosen. These profiles are depicted in Fig. 8(a), (b) and (c). It should be noted again that the base thickness of these disks are small compared to their diameters to justify the plane stress assumption. The convex disk profile (D1) in Fig. 8(a) is obtained by choosing $n = 0.96$ and $k = 0.5$. The disk profile (D2) shown in Fig. 8(b) is linear and corresponds to the geometric parameters $n = 0.8$ and $k = 1.0$. Fig. 8(c)

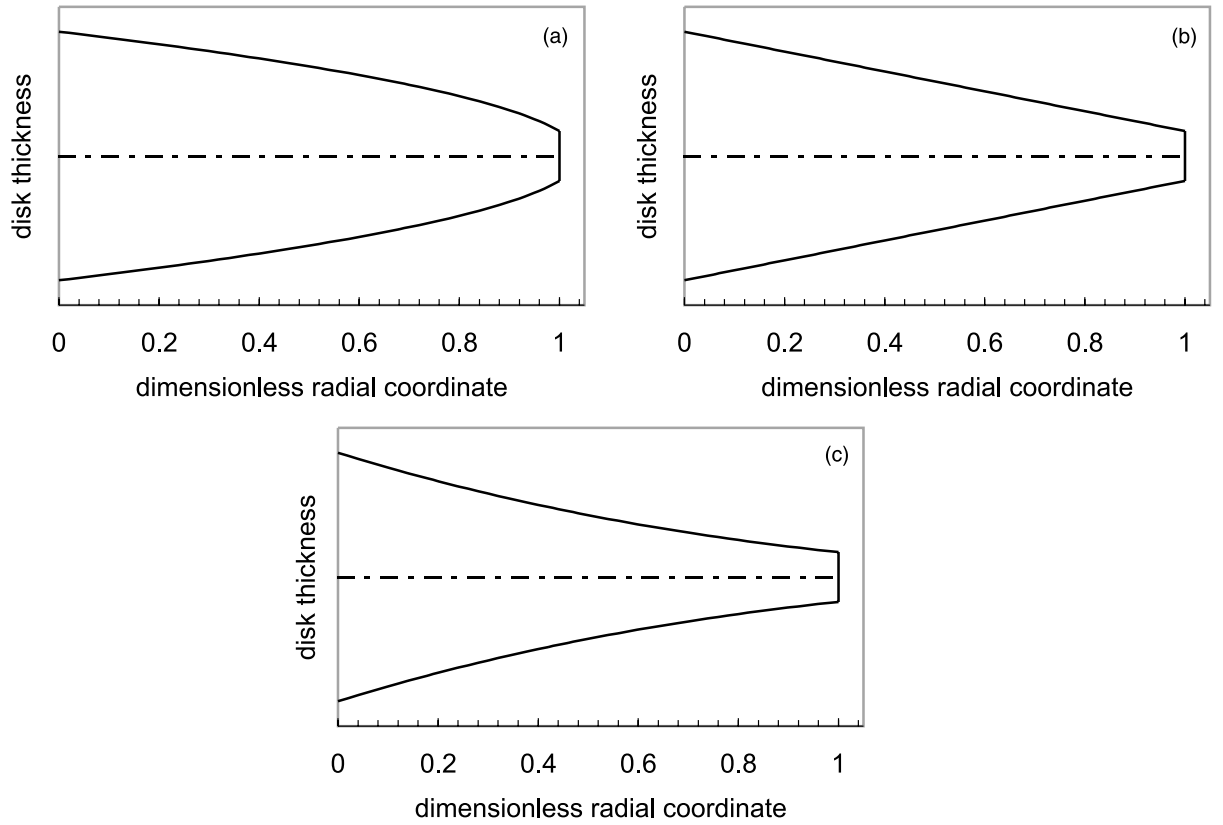

Fig. 8. Variable thickness disk profiles for (a) $n = 0.96$ and $k = 0.5$; (b) $n = 0.8$ and $k = 1.0$; (c) $n = 0.4151965$ and $k = 3.0$.

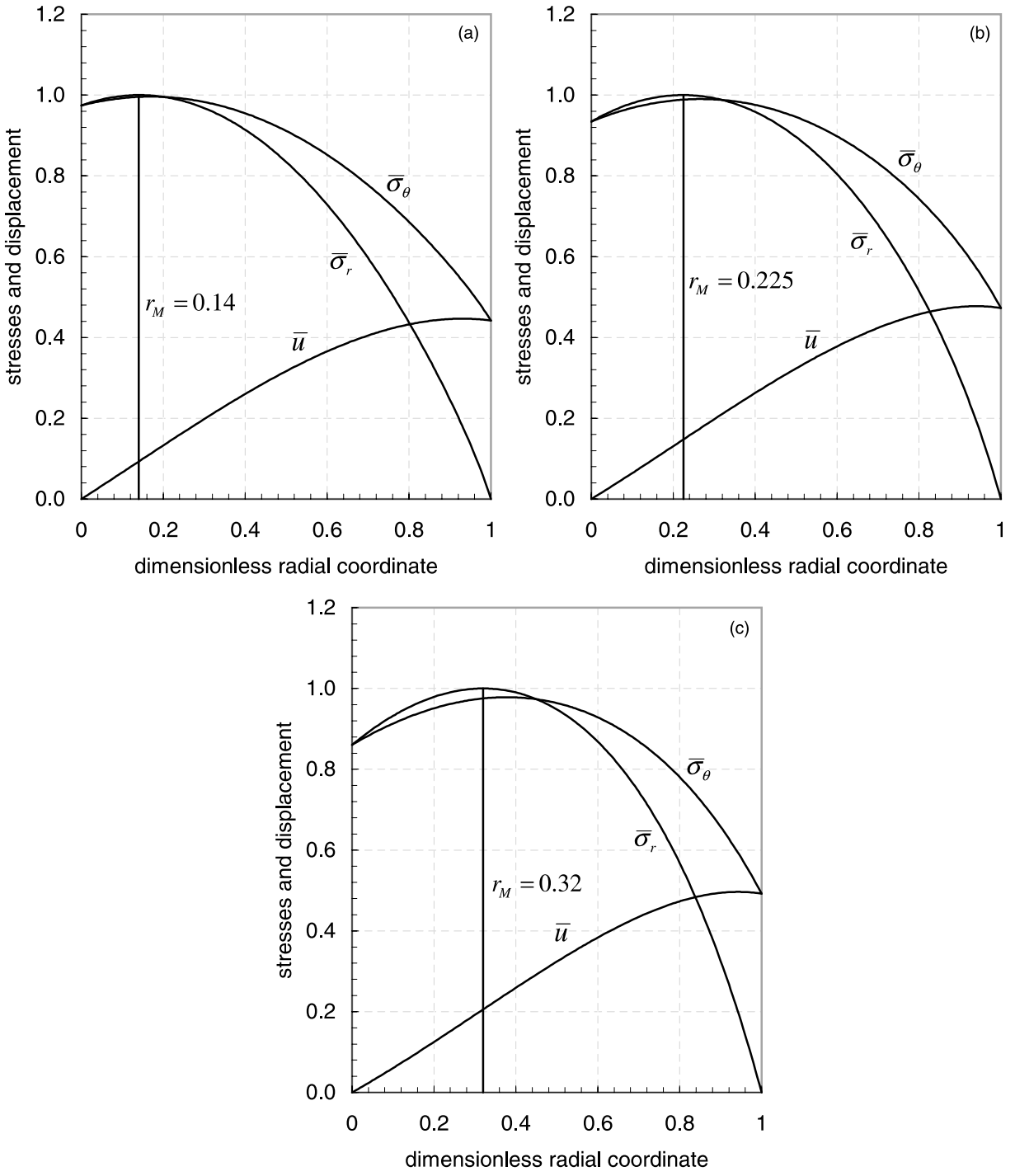

Fig. 9. Elastic stresses and deformations of variable thickness rotating solid disks for (a) $n = 0.96$ and $k = 0.5$; (b) $n = 0.8$ and $k = 1.0$; (c) $n = 0.4151965$ and $k = 3.0$.

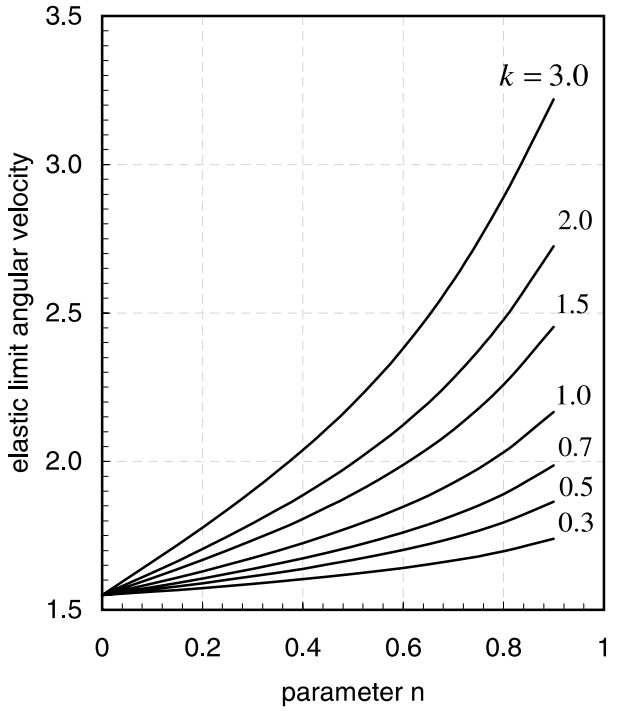

Fig. 10. Variation of elastic limit angular velocity with the thickness reduction for rotating variable thickness solid disks.

shows a concave disk profile (D3) which is obtained by setting $n = 0.4151965$ and $k = 3.0$. With these values of the geometric parameters each of the disks has 80% thickness reduction at the edge. Elastic limit angular velocities for these variable thickness solid disks are computed as $\Omega_1 = 1.923286$ for disk D1, 2.030323 for D2 and 2.060089 for D3. The corresponding stresses and displacements are plotted in Fig. 9(a), (b) and (c) for disks D1, D2 and D3, respectively. These figures reveal that, unlike uniform thickness solid disk, the radial stress in these variable thickness disks is the largest stress reaching its maximum value somewhere inside the disk not at the axis. The radial location of $d\bar{\sigma}_r/d\bar{r} = 0$ designated by $\bar{r}_M$ in Fig. 9, moves away from the axis of the disk as the disk mass decreases. This behavior of variable thickness rotating solid disks as discussed in (Eraslan and Orcan, 2002) is important because the plastic deformation should start at a radial position corresponding to $d\bar{\sigma}_r/d\bar{r} = 0$ inside the disk and will propagate in both directions as the angular velocity is increased. Fig. 10 displays the variation of elastic limit angular velocity for solid disks with thickness reduction using k as a parameter. As seen in Fig. 10, the limit angular velocity increases with decreasing disk thickness at the edge as well as decreasing mass of the disk.

3. Inelastic solution and fully plastic limit angular velocities

In the case of plane stress ($\bar{\sigma}_z = 0$), von Mises yield condition for inelastic deformations of the disk is

$$\bar{\sigma}_y = \sqrt{\bar{\sigma}_r^2 - \bar{\sigma}_r\bar{\sigma}_\theta + \bar{\sigma}_\theta^2} \tag{3.1}$$

assuming nonlinear strain hardening material behavior in the form of Swift's hardening law

$$\bar{\sigma}_y = \left(1 + H\bar{\epsilon}_{EQ}\right)^{1/m} \tag{3.2}$$

where $H = \eta\sigma_0/E$ represents normalized hardening parameter, η hardening parameter, $\bar{\epsilon}_{\mathrm{EQ}}$ normalized equivalent plastic strain and m material parameter. Note that with this form of the yield stress-equivalent strain relation, linear strain hardening can be obtained by setting $m = 1$. The inverse relation of Eq. (3.2) is

$$\bar{\epsilon}_{\mathrm{EQ}} = \left(\bar{\sigma}_y^{\mathrm{m}} - 1\right)\frac{1}{H} \tag{3.3}$$

In terms of equivalent strain the plastic strains are defined as

$$\bar{\epsilon}_{\mathrm{r}}^{\mathrm{p}} = \frac{\bar{\epsilon}_{\mathrm{EQ}}}{\bar{\sigma}_y}\left[\bar{\sigma}_{\mathrm{r}} - \frac{1}{2}\bar{\sigma}_\theta\right] \tag{3.4}$$

$$\bar{\epsilon}_\theta^{\mathrm{p}} = \frac{\bar{\epsilon}_{\mathrm{EQ}}}{\bar{\sigma}_y}\left[\bar{\sigma}_\theta - \frac{1}{2}\bar{\sigma}_{\mathrm{r}}\right] \tag{3.5}$$

Combining Eqs. (2.5), (3.3), (3.4) and (3.5) total strains are obtained as

$$\bar{\epsilon}_{\mathrm{r}} = \frac{\bar{\sigma}_y^{\mathrm{m}} - 1}{\bar{\sigma}_y H}\left[\bar{\sigma}_{\mathrm{r}} - \frac{1}{2}\bar{\sigma}_\theta\right] + \left[\bar{\sigma}_{\mathrm{r}} - v\bar{\sigma}_\theta\right] \tag{3.6}$$

$$\bar{\epsilon}_\theta = \frac{\bar{\sigma}_y^{\mathrm{m}} - 1}{\bar{\sigma}_y H}\left[\bar{\sigma}_\theta - \frac{1}{2}\bar{\sigma}_{\mathrm{r}}\right] + \left[\bar{\sigma}_\theta - v\bar{\sigma}_{\mathrm{r}}\right] \tag{3.7}$$

Substituting total strains in the compatibility relation, Eq. (2.13), one obtains

$$\frac{\left[2H(1+v)\bar{\sigma}_y + 3(\bar{\sigma}_y^{\mathrm{m}} - 1)\right](\bar{\sigma}_\theta - \bar{\sigma}_{\mathrm{r}})}{2H\bar{\sigma}_y} - \left[\bar{r}v + \frac{\bar{r}(\bar{\sigma}_y^{\mathrm{m}} - 1)}{2H\bar{\sigma}_y}\right]\frac{\mathrm{d}\bar{\sigma}_{\mathrm{r}}}{\mathrm{d}\bar{r}} + \left[\bar{r} + \frac{\bar{r}(\bar{\sigma}_y^{\mathrm{m}} - 1)}{H\bar{\sigma}_y}\right]\frac{\mathrm{d}\bar{\sigma}_\theta}{\mathrm{d}\bar{r}}$$
$$- \left\{\frac{\bar{r}\left[1 + (m-1)\bar{\sigma}_y^{\mathrm{m}}\right](\bar{\sigma}_{\mathrm{r}} - 2\bar{\sigma}_\theta)}{2H\bar{\sigma}_y^2}\right\}\frac{\mathrm{d}\bar{\sigma}_y}{\mathrm{d}\bar{r}} = 0 \tag{3.8}$$

The stresses are expressed in terms of the stress function $Y(\bar{r})$ by making use of Eqs. (2.9) and (2.19). The first-order derivatives of $\bar{\sigma}_\theta$ and $\bar{\sigma}_y$ contain second-order derivatives of Y. They are evaluated separately as

$$\frac{\mathrm{d}\bar{\sigma}_y}{\mathrm{d}\bar{r}} = \frac{N_1}{2\bar{\sigma}_y} - \frac{N_2}{2\bar{\sigma}_y}\left[N_3 + \frac{1}{\bar{h}}\frac{\mathrm{d}^2 Y}{\mathrm{d}\bar{r}^2}\right] \tag{3.9}$$

$$\frac{\mathrm{d}\bar{\sigma}_\theta}{\mathrm{d}\bar{r}} = N_3 + \frac{1}{\bar{h}}\frac{\mathrm{d}^2 Y}{\mathrm{d}\bar{r}^2} \tag{3.10}$$

where

$$N_1 = (2\bar{\sigma}_{\mathrm{r}} - \bar{\sigma}_\theta)\frac{\mathrm{d}\bar{\sigma}_{\mathrm{r}}}{\mathrm{d}\bar{r}} \tag{3.11a}$$

$$N_2 = \bar{\sigma}_{\mathrm{r}} - 2\bar{\sigma}_\theta \tag{3.11b}$$

$$N_3 = 2\Omega^2\bar{r} - \frac{1}{\bar{h}^2}\frac{\mathrm{d}\bar{h}}{\mathrm{d}\bar{r}}\frac{\mathrm{d}Y}{\mathrm{d}\bar{r}} \tag{3.11c}$$

Substituting Eqs. (3.9) and (3.10) in Eq. (3.8) and simplifying gives

$$\frac{[2H(1+\nu)\bar{\sigma}_y+3N_5]}{2H\bar{\sigma}_y}(\bar{\sigma}_\theta-\bar{\sigma}_\mathrm{r})+N_3\bar{r}\left[1+\frac{N_5}{H\bar{\sigma}_y}\right]+\frac{\bar{r}N_2N_4}{4H\bar{\sigma}_y^3}[N_2N_3-N_1]-\left[\bar{r}\nu+\frac{\bar{r}N_5}{2H\bar{\sigma}_y}\right]\frac{\mathrm{d}\bar{\sigma}_\mathrm{r}}{\mathrm{d}\bar{r}}+\left[\frac{\bar{r}}{\bar{h}}+\frac{\bar{r}N_5}{\bar{h}H\bar{\sigma}_y}+\frac{\bar{r}N_2^2N_4}{4H\bar{h}\bar{\sigma}_y^3}\right]\frac{\mathrm{d}^2Y}{\mathrm{d}\bar{r}^2}=0 \tag{3.12}$$

in which

$$N_4=(m-1)\bar{\sigma}_y^\mathrm{m}+1 \tag{3.13a}$$

$$N_5=\bar{\sigma}_y^\mathrm{m}-1 \tag{3.13b}$$

If the radial, circumferential and yield stresses are substituted from Eqs. (2.9), (2.10) and (3.1), respectively, in Eq. (3.12), the result can be cast into the general form given by Eq. (2.38). The numerical solution is obtained as described in the previous section.

A run is performed to compute the plastic limit angular velocity of a linearly hardening rotating uniform thickness solid disk by taking $H=0.5$, $\nu=1/3$, $m=1$ and setting $n=0$. Six iterations were performed to reach the convergence yielding $\Omega_2=2.117331$. Gamer (1984) used Tresca's yield condition, its associated flow rule and assumed linear strain hardening material behavior to estimate the plastic limit angular velocity of a rotating uniform thickness solid disk. He obtained a consistent closed form solution to his model and calculated the plastic limit angular velocity as $\Omega_2=2.08043$, by using the same hardening parameter

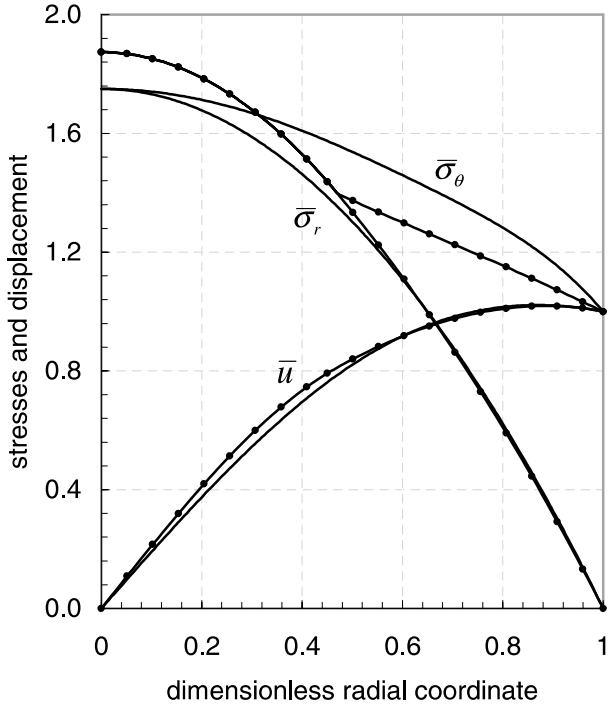

Fig. 11. Comparison of inelastic stresses and displacements by analytical Tresca solution from (Gamer, 1984) for rotating constant thickness solid disk. Dots represent analytical solution.

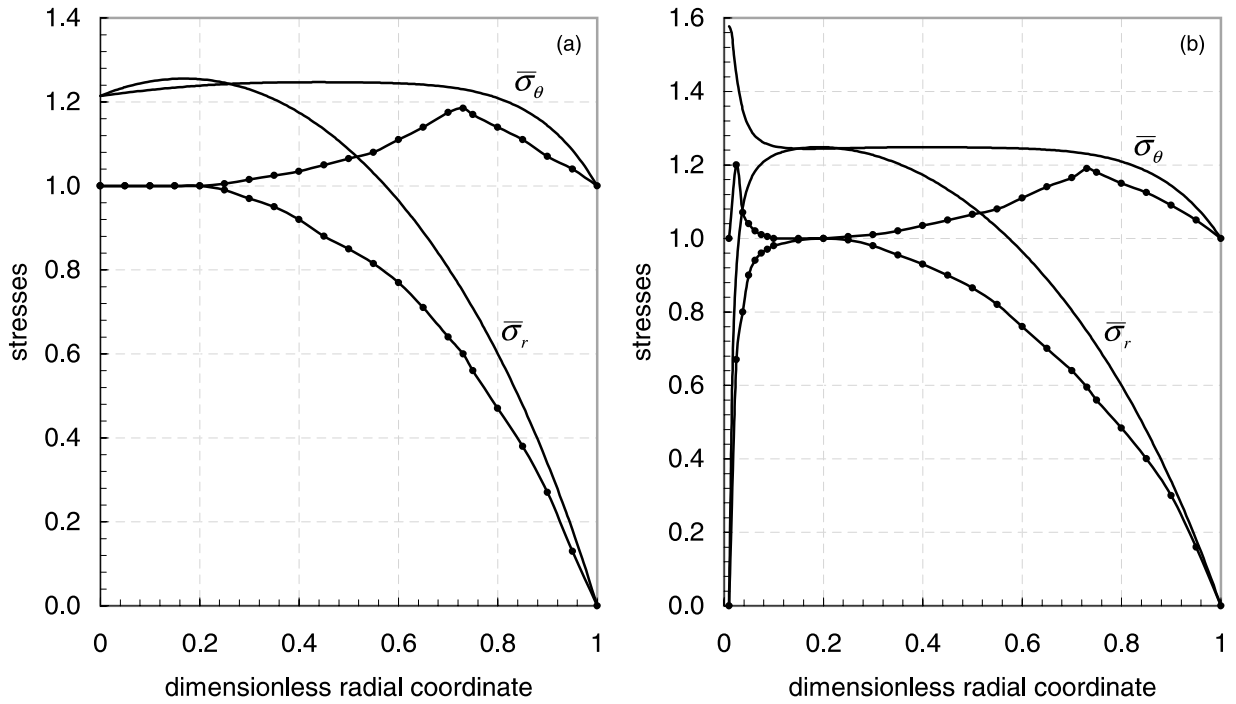

Fig. 12. Comparison of inelastic stresses by the solution of Ma et al. (2001) for (a) rotating linearly varying thickness solid disk, (b) linearly varying thickness annular disk of inner radius $\bar{r}_0 = 0.01$. Dots represent the results of Ma et al.

and Poisson's ratio. Although a different yield condition is used in this work, the result obtained here is in good agreement with that of Gamer. Furthermore, it is known that plastic limit angular velocities calculated by von Mises yield condition are slightly higher than those of Tresca (Rees, 1999). The stresses and displacement corresponding to the fully plastic state are compared to Gamer's analytical solution in Fig. 11. Although limit angular velocities are slightly different, a good agreement is obtained especially in radial stress and displacement.

Before the results of variable thickness disks are given, another comparison is made with the literature. Ma et al. (2001) computed the inelastic deformation of linearly decreasing thickness annular and solid disks, each of which corresponding to 33% thickness reduction at the edge. These disks can be studied in this work by taking $n = 2/3$ and $k = 1.0$. In addition, we set $H = 0.5$, $v = 1/3$ and $m = 3$ to simulate nonlinear hardening material behavior. Fig. 12(a) compares the results of rotating solid disk of linearly varying thickness. The agreement is very poor. This is because Ma et al. computed constant stresses in the central portion of the disk. Substituting $\bar{h}(\bar{r}) = (1 - 2/3\bar{r})$ and $\bar{\sigma}_r = \bar{\sigma}_\theta = C$, where C is a constant, in the equation of motion, Eq. (2.2), reveals

$$C = \frac{\Omega^2 \bar{r}}{2}(3 - 2\bar{r})$$

This result is contradictory to $\bar{\sigma}_r = \bar{\sigma}_\theta = \text{constant}$. Thus, their estimations fail to satisfy the equation of motion in the regions of constant radial and circumferential stresses. The results of the stresses in rotating annular disk of inner radius $\bar{r}_0 = 0.01$ are compared with those of Ma et al. in Fig. 12(b). Again, the agreement is very poor.

Using the parameters $H = 0.5$, $v = 1/3$ and $m = 3$ the stresses and displacement in rotating solid disks D1, D2 and D3 in the fully plastic state are calculated and the results are presented in Fig. 13(a), (b) and (c),

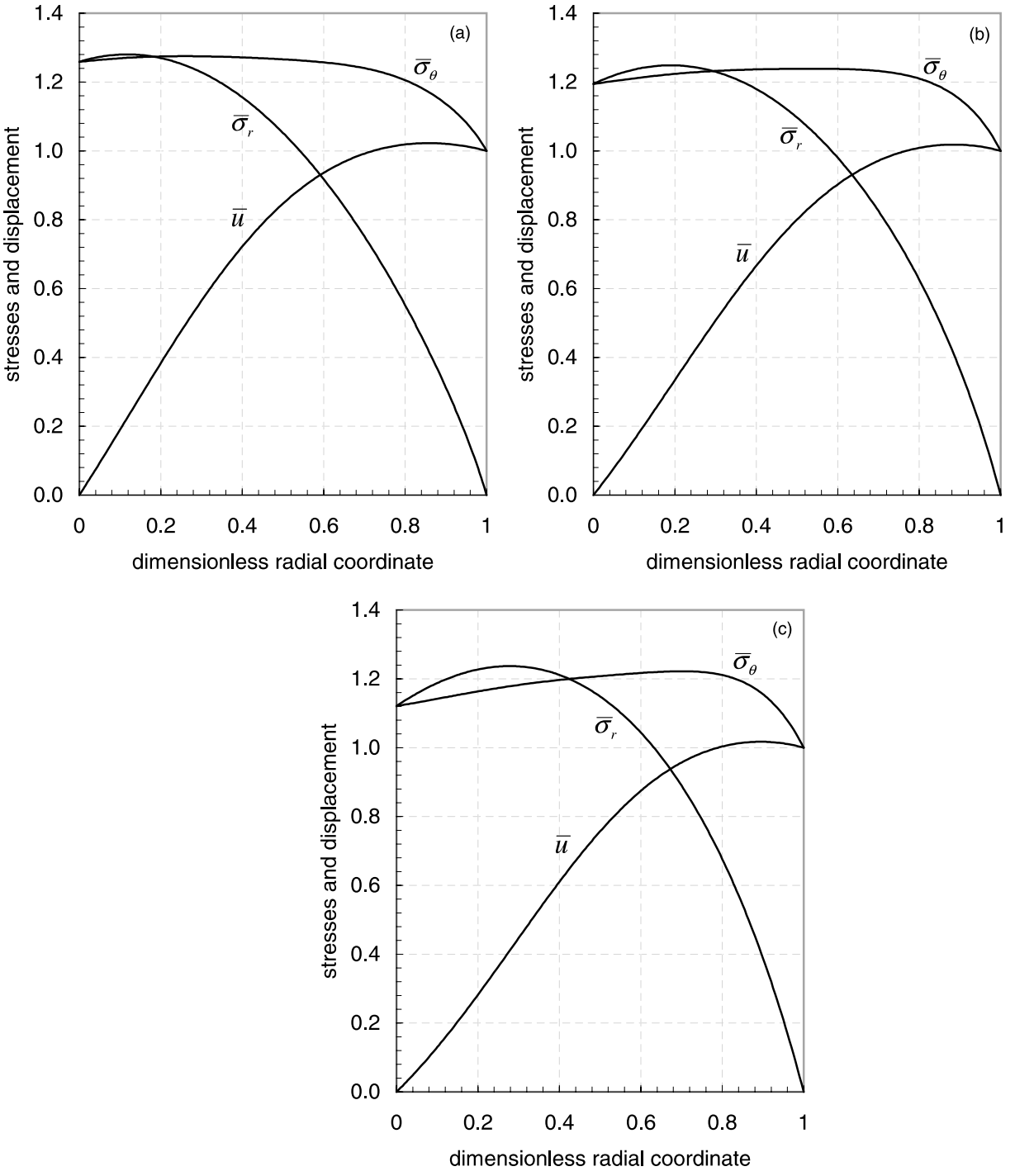

Fig. 13. Inelastic stresses and displacements in rotating variable thickness solid disks for (a) $n = 0.96$ and $k = 0.5$; (b) $n = 0.8$ and $k = 1.0$; (c) $n = 0.4151965$ and $k = 3.0$.

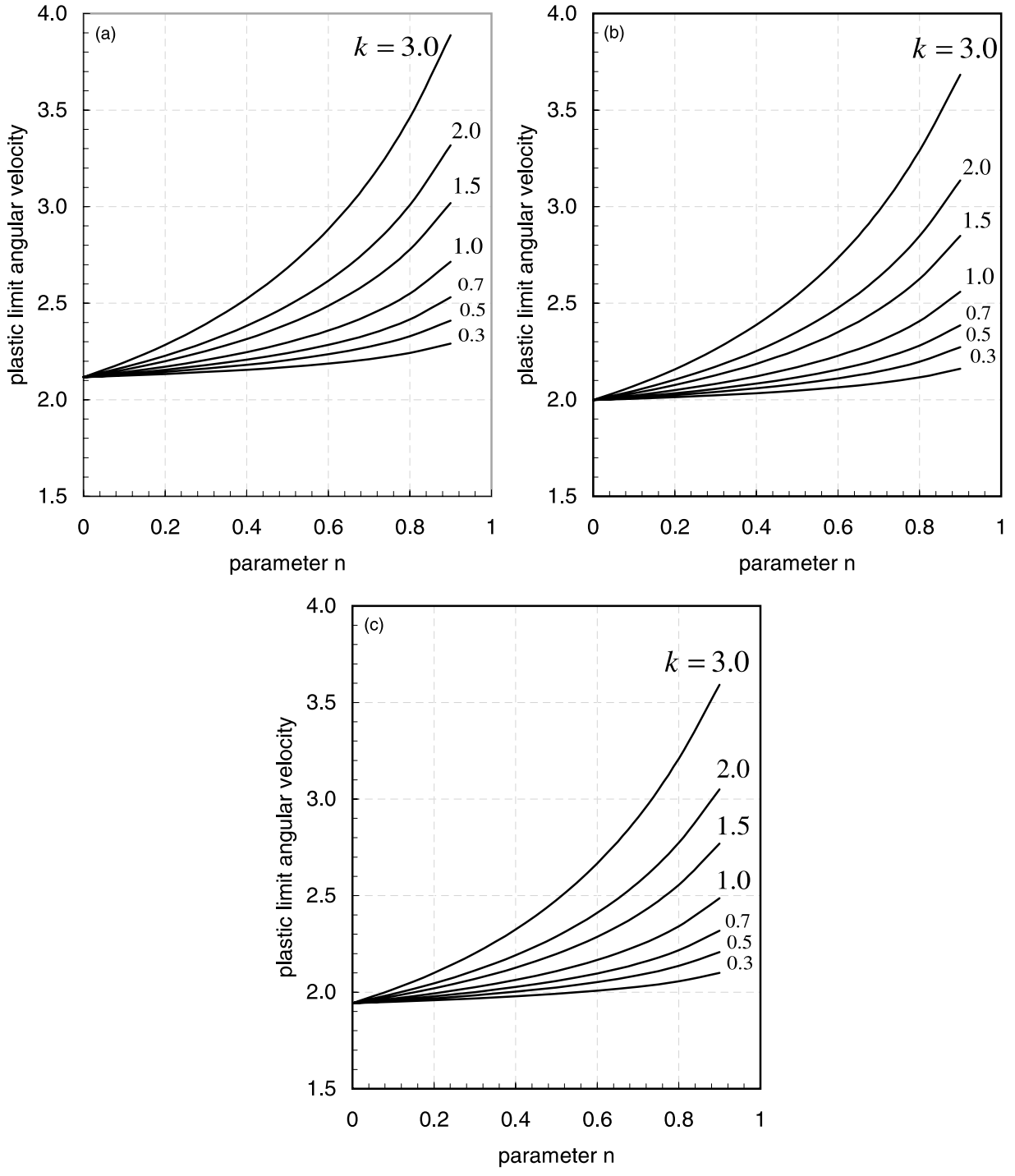

Fig. 14. Variation of plastic limit angular velocity in variable thickness solid disks with (a) linear hardening ($m = 1$), (b) nonlinear hardening ($m = 2$) and (c) nonlinear hardening ($m = 3$).

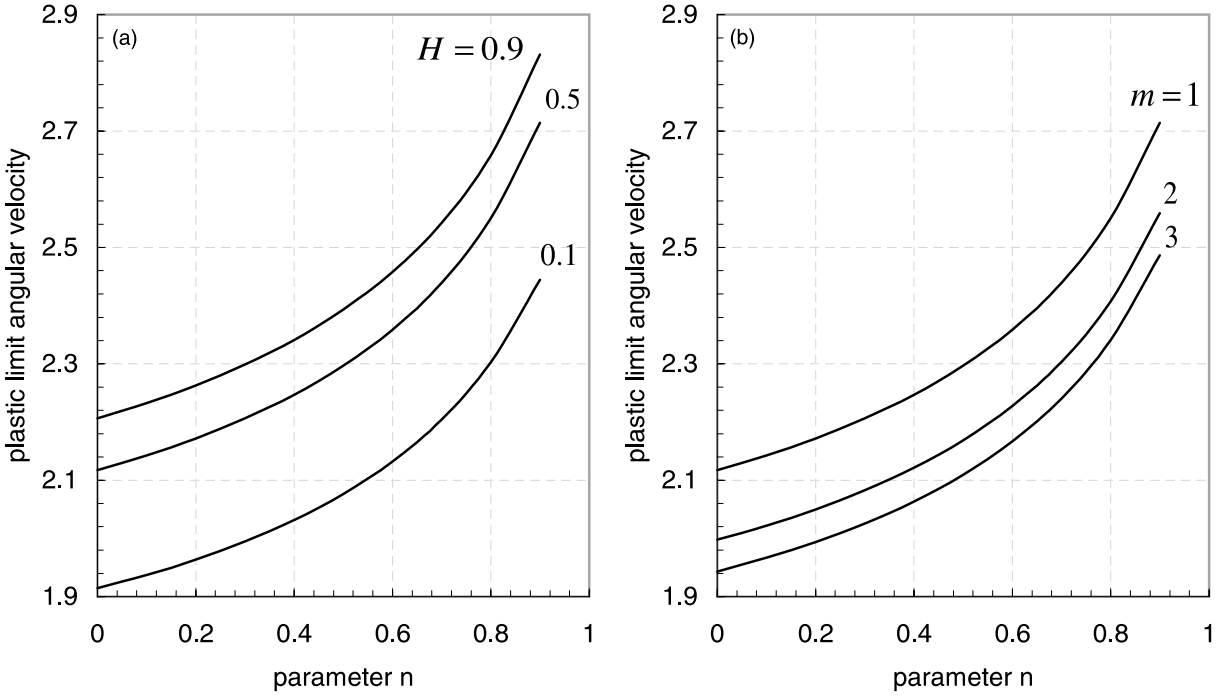

Fig. 15. Effect of (a) the hardening parameter H, (b) the material parameter m on the calculated plastic limit angular velocities.

respectively. The plastic limit angular velocities for these disks are obtained as $\Omega_2 = 2.274888$ for D1, 2.341080 for D2, and 2.346266 for disk D3. As seen in Fig. 13, the radial stress is the largest stress in these disks and the radial position of $d\bar{\sigma}_r/d\bar{r} = 0$ moves away from the axis as the disk mass decreases.

Variation of plastic limit angular velocities with disk thickness reduction is displayed in Fig. 14(a), (b) and (c) using k as a parameter for different material parameters m. Fig. 14(a) is obtained for $m = 1$ which corresponds to linear hardening material behavior. Fig. 14(b) and (c) correspond to $m = 2$ and $m = 3$, respectively, simulating nonlinear hardening material.

The effect of hardening parameter H on the plastic limit angular velocities is illustrated in Fig. 15(a) for linear hardening ($m = 1$). Plastic limit angular velocities increase as H is increased. Finally, Fig. 15(b) shows Ω vs. n using $H = 0.5$ for different material parameters m. The largest limit angular velocities are obtained for the linear hardening material and it is observed that as m increases limit angular velocities decrease.

4. Concluding remarks

Elastic stresses, displacements and limit angular velocities have been calculated for rotating variable thickness annular disks, annular disks with rigid inclusion and solid disks. Variable thickness rotating annular disks and annular disks with rigid inclusion yielded stress profiles similar to those of constant thickness ones with magnitudes smaller than the corresponding constant thickness disks at the same angular velocity. In contrast, the deformation behavior of variable thickness rotating solid disks differed significantly from constant thickness disks. The radial stress was found to be the largest principal stress and reached a maximum at a radial position inside the disk, not at the axis as in constant thickness solid disk. The location of the maximum radial stress moved away from the axis as the disk mass decreased for the

same thickness reduction at the edge. Nevertheless, elastic limit angular velocities were found to increase with increasing disk thickness reduction and with decreasing disk mass for all disks.

Inelastic deformations and plastic limit angular velocities have been computed using von Mises yield criterion and its flow rule for linear and nonlinear hardening rotating solid and annular disks. A comparison with Tresca's yield condition showed that the plastic limit angular velocity obtained by von Mises yield condition is slightly higher than Tresca for the linear hardening material. Plastic limit angular velocities have been found to be affected by the shape of the disk profile significantly. The reduction in the disk thickness increased plastic limit angular velocities. Lower plastic limit angular velocities have been obtained for nonlinearly hardening rotating solid disks.

Appendix A. Displacement formulation and solution

Substituting the elastic strains from Eqs. (2.6) and (2.7) in Eqs. (2.3) and (2.4) and solving for the stresses, the stress-displacement relations are obtained as

$$\bar{\sigma}_r(\bar{r}) = \frac{v\bar{u}(r) + \bar{r}\bar{u}'(\bar{r})}{\bar{r}(1-v^2)} \tag{A.1}$$

$$\bar{\sigma}_\theta(\bar{r}) = \frac{\bar{u}(r) + \bar{r}v\bar{u}'(\bar{r})}{\bar{r}(1-v^2)} \tag{A.2}$$

Substituting these stresses in the equation of motion, Eq. (2.2), and simplifying the following differential equation for the dimensionless radial displacement $\bar{u}$ is obtained.

$$\frac{d^2\bar{u}}{d\bar{r}^2} + \left[\frac{1}{\bar{r}} + \frac{\bar{h}'}{\bar{h}}\right]\frac{d\bar{u}}{d\bar{r}} - \left[\frac{1}{\bar{r}^2} - \frac{v\bar{h}'}{\bar{r}\bar{h}}\right]\bar{u} = g(\bar{r}) \tag{A.3}$$

in which

$$g(\bar{r}) = -\left(1-v^2\right)\Omega^2\bar{r} \tag{A.4}$$

Hence the homogeneous equation is obtained by setting $g = 0$. One solution to the homogeneous equation is found to be

$$y_1(\bar{r}) = \bar{r}\mathsf{F}(a,b,c,n\bar{r}) \tag{A.5}$$

where $\mathsf{F}(\alpha,\beta,\gamma,x)$ is the hypergeometric function defined by Eq. (2.20) and a, b, c are

$$\begin{aligned} a &= 1 + \frac{k}{2} - \frac{1}{2}\sqrt{k^2 + 4(1-kv)} \\ b &= 1 + \frac{k}{2} + \frac{1}{2}\sqrt{k^2 + 4(1-kv)} \\ c &= 3 \end{aligned} \tag{A.6}$$

By using the method of reduction of order the second linearly independent solution is found to be

$$y_2(\bar{r}) = y_1(\bar{r})I_1(\bar{r}) \tag{A.7}$$

where

$$I_1(\bar{r}) = \int_{\bar{r}_0}^{\bar{r}} \frac{d\xi}{\xi\bar{h}(\xi)y_1(\xi)^2} \tag{A.8}$$

Note that as in the stress function solution, this integral contains non-integrable singularity at $\bar{r}_0 = 0$, accordingly, it is valid for annular disks. The general solution for the radial displacement can be written as

$$\bar{u}(\bar{r}) = C_1 y_1(\bar{r}) + C_2 y_2(\bar{r}) + R(\bar{r}) \tag{A.9}$$

The particular integral solution $R(\bar{r})$ is obtained by the method of variation of parameters. The result is

$$R(\bar{r}) = y_1(\bar{r})\Big[I_1(\bar{r})I_2(\bar{r}) - I_3(\bar{r})\Big] \tag{A.10}$$

where

$$I_2(\bar{r}) = \int_{\bar{r}_0}^{\bar{r}} z y_1(z) g(z) \bar{h}(z)\,\mathrm{d}z \tag{A.11}$$

$$I_3(\bar{r}) = \int_{\bar{r}_0}^{\bar{r}} \int_{\bar{r}_0}^{z} \Big[z y_1(z) g(z) \bar{h}(z)\Big] \left[\frac{1}{\xi \bar{h}(\xi) y_1(\xi)^2}\right] \mathrm{d}\xi\,\mathrm{d}z \tag{A.12}$$

Appendix B. Alternate solution for the stress function formulation

To solve the linear differential equation, Eq. (2.14), we first substitute $\bar{h} = (1 - n\bar{r})^k$ and $\bar{h}' = -kn(1 - n\bar{r})^{k-1}$ in this equation, then introduce a new variable $z = 1 - n\bar{r}$ and the transformation $Y(\bar{r}) = (1 - z)G(z)/n$ to obtain

$$z(1-z)\frac{\mathrm{d}^2 G}{\mathrm{d}z^2} - [k + (3-k)z]\frac{\mathrm{d}G}{\mathrm{d}z} + k(1-v)G = -\frac{1}{n^2}\left[(3+v)\Omega^2(1-z)z^{k+1}\right] \tag{B.1}$$

Eq. (B.1) is a hypergeometric differential equation with the homogeneous solution (Abramowitz and Stegun, 1966)

$$G(z) = C_1 g_1(z) + C_2 g_2(z) \tag{B.2}$$

where C_1 and C_2 are arbitrary integration constants and

$$\begin{aligned} g_1(z) &= \mathsf{F}(a, b, c, z) \\ g_2(z) &= z^{1+k}\mathsf{F}(a - c + 1, b - c + 1, 2 - c, z) \\ a &= 1 - \frac{k}{2} - \frac{1}{2}\sqrt{k^2 + 4(1 - kv)} \\ b &= 1 - \frac{k}{2} + \frac{1}{2}\sqrt{k^2 + 4(1 - kv)} \\ c &= -k \end{aligned} \tag{B.3}$$

The function $\mathsf{F}(\alpha, \beta, \gamma, x)$ in the above equation is the hypergeometric function described by Eq. (2.20). The general solution for the stress function $Y(\bar{r})$ takes the form

$$Y(\bar{r}) = \bar{r}\Big[C_1 \mathsf{F}(a, b, c, 1 - n\bar{r}) + C_2(1 - n\bar{r})^{1+k}\mathsf{F}(a - c + 1, b - c + 1, 2 - c, 1 - n\bar{r})\Big] + R(\bar{r}) \tag{B.4}$$

where $R(\bar{r})$ is the particular solution which can be obtained using variation of parameters. Since the function $\mathsf{F}(a, b, c, 1 - n\bar{r})$ is not finite at the axis of the disk, this solution is valid for annular disks.

Appendix C. Note on the evaluation of hypergeometric functions

The hypergeometric function defined by the series given by Eq. (2.20) converges slowly. At first sight, it may be thought that summing up several terms of the series would be sufficient to get the correct numerical value of the function. But this may not be true. As $|x| \to 1$ the rate of convergence is extremely slow. For example, to get the true value 13.3244385 of the hypergeometric function $\mathsf{F}(0.9, 0.9, 1.3, 0.99)$ 1892 terms should be added. Care must be exercised in calculating hypergeometric functions especially when $|x|$ approaches to 1. To be able to add such a large number of terms, each term should be factorized. For example, the fourth term T_4 in the series is obtained by the following calculation sequence:

$$t_1 = \frac{\alpha}{\gamma}; \quad t_2 = \frac{\alpha+1}{\gamma+1}; \quad t_3 = \frac{\alpha+2}{\gamma+2}; \quad \hat{t}_1 = \frac{\beta}{1}; \quad \hat{t}_2 = \frac{\beta+1}{2}; \quad \hat{t}_3 = \frac{\beta+2}{3} \tag{C.1}$$

Then

$$T_4 = \frac{\alpha(\alpha+1)(\alpha+2)\beta(\beta+1)(\beta+2)}{\gamma(\gamma+1)(\gamma+2)3!}x^3 = t_1 \cdot t_2 \cdot t_3 \cdot \hat{t}_1 \cdot \hat{t}_2 \cdot \hat{t}_3 \cdot x \cdot x \cdot x \tag{C.2}$$

This calculation procedure avoids evaluation of factorials of large numbers which is practically not possible. Furthermore, the following linear transformation (Abramowitz and Stegun, 1966) is useful in increasing the rate of convergence of the series:

$$F(\alpha, \beta, \gamma, x) = (1-x)^{\gamma-\alpha-\beta} F(\gamma-\alpha, \gamma-\beta, \gamma, x) \tag{C.3}$$

References

Abramowitz, M., Stegun, A.I. (Eds.), 1966. Handbook of Mathematical Functions. US Government Printing Office, Washington DC (fifth ed.).

Calladine, C.R., 1969. Engineering plasticity. Pergamon Press, Oxford.

Eraslan, A.N., Orcan, Y., 2002. On the rotating elastic–plastic solid disks of variable thickness having concave profiles. Int. J. Mech. Sci. (in press).

Gamer, U., 1984. Elastic-plastic deformation of the rotating solid disk. Ingenieur-Archiv. 54, 345–354.

Güven, U., 1998. Elastic–plastic stress distribution in rotating hyperbolic disk with rigid inclusion. Int. J. Mech. Sci. 40, 97–109.

Ma, G., Hao, H., Miyamoto, Y., 2001. Limit angular velocity of rotating disc with unified yield criterion. Int. J. Mech. Sci. 43, 1137–1153.

Rees, D.W.A., 1990. The mechanics of solids and structures. McGraw-Hill, New York.

Rees, D.W.A., 1999. Elastic-plastic stresses in rotating discs by von Mises and Tresca. ZAMM Z. Angew. Math. Mech. 79, 281–288.

Timoshenko, S., Goodier, J.N., 1970. Theory of elasticity, third ed. McGraw-Hill, New York.

You, L.H., Long, S.Y., Zhang, J.J., 1997. Perturbation solution of rotating solid disks with nonlinear strain-hardening. Mech. Res. Commun. 24, 649–658.

You, L.H., Zhang, J.J., 1999. Elastic–plastic stresses in a rotating solid disk. Int. J. Mech. Sci. 41, 269–282.

You, L.H., Tang, Y.Y., Zhang, J.J., Zheng, C.Y., 2000. Numerical analysis of elastic-plastic rotating disks with arbitrary variable thickness and density. Int. J. Solids Struct. 37, 7809–7820.